ACS APPLIED MATERIALS & INTERFACES

Research Article

www.acsami.org

Soft Matter Lubrication: Does Solid Viscoelasticity Matter?

Carmine Putignano*,†,‡ and Daniele Dini†

†Department of Mechanical Engineering, Imperial College London, London SW7 2AZ, United Kingdom

‡Department of Mechanics, Mathematics and Management, Politecnico di Bari, Bari 70126, Italy

Supporting Information

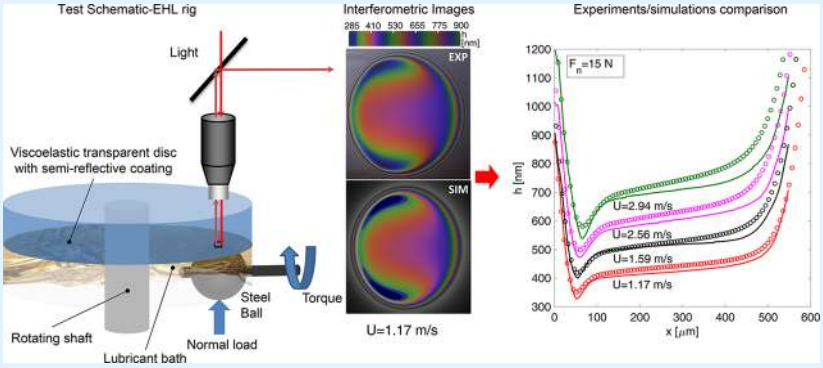

ABSTRACT: Classical lubrication theory is unable to explain a variety of phenomena and experimental observations involving soft viscoelastic materials, which are ubiquitous and increasingly used in e.g. engineering and biomedical applications. These include unexpected ruptures of the lubricating film and a friction−speed dependence, which cannot be elucidated by means of conventional models, based on time-independent stress−strain constitutive laws for the lubricated solids. A new modeling framework, corroborated through experimental measurements enabled via an interferometric technique, is proposed to address these issues: Solid/fluid interactions are captured thanks to a coupling strategy that makes it possible to study the effect that solid viscoelasticity has on fluid film lubrication. It is shown that a newly defined visco-elasto-hydrodynamic lubrication (VEHL) regime can be experienced depending on the degree of coupling between the fluid flow and the solid hysteretic response. Pressure distributions show a marked asymmetry with a peak at the flow inlet, and correspondingly, the film thickness reveals a pronounced shrinkage at the flow outlet; friction is heavily influenced by the viscoelastic hysteresis which is experienced in addition to the viscous losses. These features show significant differences with respect to the classical elasto-hydrodynamic lubrication (EHL) regime response that would be predicted when solid viscoelasticity is neglected. A simple yet powerful criterion to assess the importance of viscoelastic solid contributions to soft matter lubrication is finally proposed.

KEYWORDS: *lubrication, viscoelasticity, friction*

1. INTRODUCTION

Soft matter mechanics has recently become the focal point of much research in engineering and material science. This is driven by the continuously increasing demand for new polymers,[1,2] soft tissues,[3] biomedical implants,[4] biomimetic solutions,[5,6] and smart devices.[7] Materials belonging to this class are usually characterized by a range of outstanding properties in terms of cost, versatility, and biocompatibility. However, at the same time, because of the strongly time-dependent constitutive laws governing their behavior, their mechanical response is often difficult to predict, and indeed, a comprehensive theoretical framework to tackle this issue is still missing. A particularly high level of intricacy is reached when soft bodies come into contact: the presence of rough interfaces and the need to resolve interactions between asperities exacerbates the problem's complexity. Furthermore, at the contact interface, different phases may exist, including gases and fluids, and strong coupling effects have to be accounted for in a fully multiphysics investigation.

Indeed, because of both its theoretical and technological relevance, the case of the lubrication of soft bodies exhibiting a time-dependent viscoelastic behavior is particularly interesting. The mechanics of viscoelastic dry contacts has attracted a large number of investigations applying analytical,[8,9] numerical,[10,11,29] and experimental[12,13] methodologies. However, upon consideration of a lubricated interface in the presence of soft viscoelastic materials, limited research has been carried out both experimentally and theoretically to shed light on the mechanisms governing such interactions. In particular, in spite of the development of interesting analyses that show the effect of viscoelasticity in two-dimensional contacts,[14−17] also accounting for the role of surface roughness in a statistical sense,[14] theoretical and computational efforts to study three-dimensional contacts and to determine the effect of solid

Received: June 29, 2017
Accepted: November 6, 2017
Published: November 7, 2017

DOI: 10.1021/acsami.7b09381
ACS Appl. Mater. Interfaces 2017, 9, 42287−42295

viscoelasticity on lubrication regime are lacking. As a result, lubrication science, as so far developed for time-independent elastic,[18,19] hyper-elastic,[21] and elasto-plastic[22] rheologies of the lubricated bodies, cannot explain a variety of natural phenomena and experimental observations. An example is given by interferometric tests carried out on PMMA recently reported by Marx and co-workers,[23] which reveal film thickness maps and contact patches whose shapes and values are unexpectedly different from conventional Hertzian-like contact configurations. In particular, a marked shrinkage at the flow outlet, depending on the flow speed, is shown. Additional surprising experimental evidence linked to the interplay between solids and fluids in soft contact problems is provided in ref 24 where, in the presence of strongly viscoelastic materials, the rupture of the fluid film is shown to occur at the flow inlet of the lubricated interface. This suggests that a point of minimum for the film thickness occurs there: Such a result is very hard to explain in the absence of time-dependent deformations, and is unexpected in classical lubrication, where, because of the flow conservation, a minimum is usually predicted close to the flow outlet. Furthermore, standard lubrication models predict a friction−speed dependence that follows the so-called Stribeck curve: Boundary and mixed lubrication regimes experienced at low and moderate speeds are replaced, at larger speeds, by elasto-hydrodynamic lubrication (EHL) and hydrodynamic (HD) regimes, where friction is controlled by viscous losses in the fluid and depends linearly on the logarithm of the speed.[18] This approach neglects completely the hysteretic dissipation that occurs inside the lubricated body if the material is viscoelastic. However, such a contribution, as experimentally shown in the literature,[25] may play a significant role and strongly modify the Stribeck curve previously described.

Building up a theoretical framework for soft matter lubrication is not only fundamental to fully understand such experimental observations, but also has significant implications in allowing for many systems and applications to be studied. As sketched also in Figure 1, these include the vast field of lubrication in soft biological systems. This is, for example, the case of the tree frog's outstanding ability to adhere on wet interfaces after lubricant film breakage. Indeed, as shown in the recent literature,[24,26] frogs' toe pads frequently slip on smooth lubricated surfaces, and regain grip only when the lubricating film breaks after a small slide. Such a mechanism cannot be explained without accounting for the real rheology of the contacting interfaces. Similarly, the interaction between soft tissues and liquids is crucial also in many other contexts, like the skin grip in the presence of wet interfaces. As shown experimentally in the literature,[27] the human fingertip gripping contact is dramatically influenced by the amount of liquid at the interface and, therefore, by the lubricating film thickness. In this respect, our study is prompted also by the fact that, in the era of touchscreens, a theoretical framework to provide better understanding of gripping and fingertip sliding mechanisms is still missing. Furthermore, we should not forget the relevance of viscoelastic lubrication when looking at the important role played in determining the efficiency in a variety of engineering components. The applications dealing with the sealing technology are particularly interesting, where, in spite of a number of accurate scientific contributions (see, e.g., ref 10), the coupling between the percolating fluid and the viscoelastic solid usually is not fully accounted for.

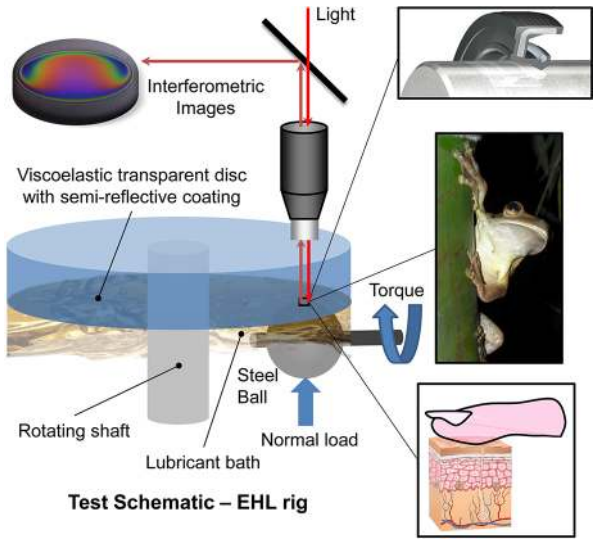

Figure 1. Lubrication of viscoelastic solids: schematic illustration of the experimentally detected film thickness and of relevant applications governed by this phenomenon.

In this paper, by means of an innovative numerical methodology that captures fluid/solid interactions, obtained by coupling a boundary element approach that deals with the solid viscoelastic deformation and a finite difference scheme used to model fluid flow dynamics, we shed light on some of the peculiarities experienced by linearly viscoelastic bodies when subjected to lubricated contact. In particular, for a simple tribosystem model, i.e., a rigid sphere in pure rolling over a viscoelastic layer, we show how non-Hertzian pressure distributions and the relative unconventional shapes for the contact film thickness can be explained by considering the actual rheology of the contacting solids. Furthermore, after providing experimental evidence for corroboration and discussing implications of our computational results, we propose a basic but effective criterion to establish when solid viscoelasticity is strongly coupled with the fluid viscous losses and has significant effects on the system response and frictional losses. The fundamental understanding gained in introducing the effect of solid viscoelasticity in the solution of lubrication problems will play an essential role in overcoming some of the limitations of classical lubrication theory and, thus, in providing a new tool to investigate the mechanisms governing some of the aforementioned phenomena.

2. MATHEMATICAL FORMULATION

In order to deal with the lubrication in the presence of deformable bodies, as schematically reproduced in Figure 2, let us focus on a scheme typical in tribology. A rigid spherical punch clamped in its center rolls, with a velocity $\mathbf{u}_b$ equal to $\mathbf{u}_b = \boldsymbol{\Omega} \times \mathbf{R}$ with $\boldsymbol{\Omega}$ and $\mathbf{R}$ being, respectively, the angular velocity and the position vector, over a viscoelastic layer sliding with a constant speed $\mathbf{u}_d$. We can assume that $\mathbf{u}_b$ and $\mathbf{u}_d$ are constant and have the same direction, i.e., $\mathbf{u}_b = u_b\mathbf{i}$ and $\mathbf{u}_d = u_d\mathbf{i}$ with $\mathbf{i}$ being the unit vector, identifying the common motion direction (corresponding to the horizontal direction in Figure 2). It is noteworthy to underline that the mathematical approach developed below is absolutely general and can be employed for any contact configuration, once the geometry of the contact and $\mathbf{u}_b$ and $\mathbf{u}_d$ are defined.

Now, the complete solution of the lubrication problem requires determination of two unknown distributions, i.e., the film thickness in the contact region and the normal interfacial stress. To this aim, it is

DOI: 10.1021/acsami.7b09381
ACS Appl. Mater. Interfaces 2017, 9, 42287−42295

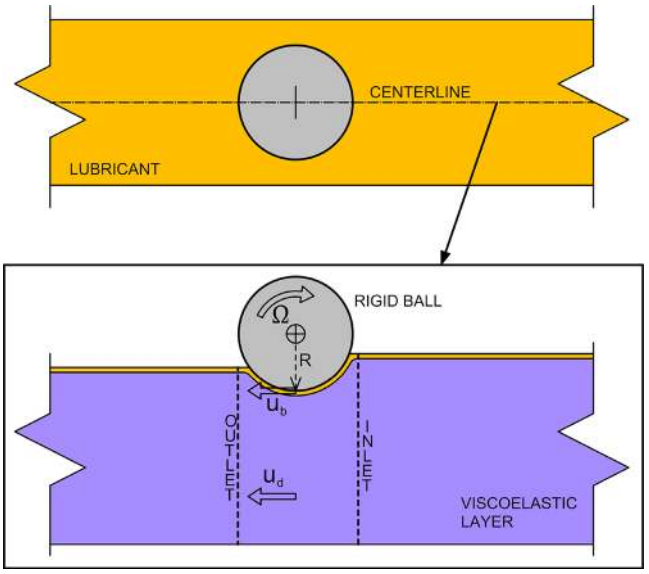

Figure 2. Schematic of the model implemented in the numerical methodology. The sphere rolls over a viscoelastic layer with a speed $\mathbf{u}_b = \boldsymbol{\Omega} \times \mathbf{R}$ with $\boldsymbol{\Omega}$ and $\mathbf{R}$ being, respectively, the constant angular velocity and the position vector. The viscoelastic layer slides with a constant speed $\mathbf{u}_d$.

necessary to couple a solver for the steady-state hydrodynamic lubrication equations with a methodology that, given the pressure distribution, provides the elastic (or viscoelastic) deformation experienced by the interacting pair. Indeed, the two aspects of the problem are coupled since the displacement of the solid surface influences the lubricating film and, consequently, the solution of the flow equations. Such a coupling is particularly strong in soft materials since deformations can be significant when compared to the fluid film thickness.

Before dealing with the problem equations, let us briefly recall how linear viscoelastic materials can be described from a mechanical point of view.[30,31] Indeed, the most general form to model the linear viscoelasticity response can be encompassed in the following relation:

$$\varepsilon(t) = \int_{-\infty}^{t} \mathrm{d}\tau\, \mathcal{J}(t-\tau)\, \dot{g}(\tau) \tag{1}$$

with $\varepsilon(t)$ being the time-dependent strain, $g(t)$ being the stress [the symbol "$\cdot$" stands for the time derivative], and the function $\mathcal{J}(t)$ being the creep function. We observe that $\mathcal{J}(t)$ must satisfy causality, and therefore, $\mathcal{J}(t<0) = 0$. It is possible to show that $\mathcal{J}(t)$ is equal to[30]

$$\begin{aligned}\mathcal{J}(t) &= \mathcal{H}(t)\left[\frac{1}{E_0} - \int_0^{+\infty} \mathrm{d}\tau\, C(\tau)\exp(-t/\tau)\right] \\ &= \mathcal{H}(t)\left[\frac{1}{E_\infty} + \int_0^{+\infty} \mathrm{d}\tau\, C(\tau)\exp(-t/\tau)\right]\end{aligned} \tag{2}$$

where $\mathcal{H}(t)$ is the Heaviside step function, the real quantities E_0 and E_∞ are, respectively, the so-called rubbery and glassy elastic moduli, $C(\tau)$ is a positive function usually referred to as the creep (or retardation) spectrum,[30] and τ is the relaxation time continuously distributed on the real axis. For employment of eq 2 to characterize any real linear viscoelastic solid, such a relation has to be discretized by writing $C(\tau) = \sum_k C_k \delta(\tau - \tau_k)$ and, thus, obtaining the following:

$$\mathcal{J}(t) = \mathcal{H}(t)\left[\frac{1}{E_0} - \sum_{k=1}^{n} C_k \exp(-t/\tau_k)\right] \tag{3}$$

where the quantities C_k and τ_k are, respectively, the creep coefficients and the relaxation times.

Furthermore, for exhaustive description of the linear viscoelasticity, it is crucial to introduce an additional quantity, that is, the so-called viscoelastic modulus of the material $E(\omega)$. Indeed, if we carry out the Fourier transform of eq 1 by introducing $\mathcal{J}(\omega) = \int \mathrm{d}t\, \mathcal{J}(t)\exp(-i\omega t)$, $\sigma(\omega) = \int \mathrm{d}t\, \sigma(t)\exp(-i\omega t)$, and $\varepsilon(\omega) = \int \mathrm{d}t\, \varepsilon(t)\exp(-i\omega t)$, we obtain $\varepsilon(\omega) = \sigma(\omega)/E(\omega)$ where $E(\omega)$ is equal to $E(\omega) = [i\omega J(\omega)]^{-1}$. By moving from eq 2, one can easily prove the *sum rule*:

$$\frac{1}{E_0} - \frac{1}{E_\infty} = \frac{2}{\pi}\int_0^\infty \mathrm{d}\omega\, \frac{1}{\omega}\,\mathrm{Im}\,\frac{1}{E(\omega)} \tag{4}$$

Now, after introducing the fundamentals of linear viscoelasticity, let us focus on the linear viscoelastic solid deformation experienced because of the indentation of such a material in a contact problem. As shown in detail in ref 11 by recalling the translational invariance of the geometrical domain and the elastic−viscoelastic correspondence principle,[30] the general linear−viscoelastic relation between the normal surface displacement $u(\mathbf{x}, t)$ and the normal interfacial stress $\sigma(\mathbf{x}, t)$ can be described by means of the following integral equation:

$$u(\mathbf{x}, t) = \int_{-\infty}^{t} \mathrm{d}\tau \int \mathrm{d}^2x'\, \mathcal{J}(t-\tau)\, \mathcal{G}(\mathbf{x}-\mathbf{x}')\, \dot{\sigma}(\mathbf{x}', \tau) \tag{5}$$

where $\mathbf{x}$ is the in-plane position vector, t is the time, and $\mathcal{G}(\mathbf{x})$ and $\mathcal{J}(t)$ are, respectively, the elastic Green's function and the creep function previously introduced. Incidentally, it should be observed that, in eq 5, the factorization of the integral equation kernel in two terms, that is, $\mathcal{G}(\mathbf{x})$ and $\mathcal{J}(t)$, is allowed because of the assumption on the rheology of the contacting solids, which are considered homogeneous linear viscoelastic.

Now, since the sliding of the viscoelastic materials occurs at the constant velocity $\mathbf{u}_d$, and neglecting any effect due to a nonuniform temperature field, we can rely on a steady-state assumption and observe that, in such a case, $\sigma(\mathbf{x}, t) = \sigma(\mathbf{x} - \mathbf{u}_d t)$, and $u(\mathbf{x}, t) = u(\mathbf{x} - \mathbf{u}_d t)$. Consequently, eq 5 can be rewritten in the following form:

$$u(\mathbf{x}) = \int \mathrm{d}^2x'\, G(\mathbf{x}-\mathbf{x}', \mathbf{u}_d)\, \sigma(\mathbf{x}') \tag{6}$$

In refs 11 and 32, the kernel $G(\mathbf{x}, \mathbf{u}_d)$, which depends only parametrically on the speed $\mathbf{u}_d$, has been proven to be equal to

$$\begin{aligned}G(\mathbf{x}, \mathbf{u}_d) = -\frac{1-\upsilon^2}{\pi}\Bigg\{&\frac{1}{E_\infty}\frac{1}{|\mathbf{x}|}\Theta\left(\frac{|\mathbf{x}|}{b}\right) + \int_0^{+\infty} \mathrm{d}\tau\, C(\tau) \\ &\int_0^{+\infty} \mathrm{d}z\, \frac{1}{|\mathbf{x} + \mathbf{u}_d\tau z|}\Theta\left(\frac{|\mathbf{x} + \mathbf{u}_d\tau z|}{b}\right)\exp(-z)\Bigg\}\end{aligned} \tag{7}$$

where $\Theta(|\mathbf{X}|/b)$ is a corrective parameter introduced to account for the viscoelastic slab thickness b and depending on the different constrains or boundary conditions set on the layer (see refs 32−34 for more details). When the contact region is much smaller than the slab thickness, the layer behaves like a half-space, and $\Theta(|\mathbf{X}|/b)$ tends to 1.

Once the Green's function $G(\mathbf{x}, \mathbf{u}_d)$ is explicitly given, for a numerical solution, eq 6 has to be discretized as a linear system.[28,36] Indeed, this strategy consists of discretizing the contact domain in N square cells and, then, assuming that in each square cell the normal stress σ is constant and equal to $\sigma_k = \sigma(\mathbf{X}_k)$, where $\mathbf{X}_k$ is the position vector of the center of the square cell D_k. Consequently, the normal displacement $u_i = u(\mathbf{X}_i)$ at the center of the i-th square cell can be expressed as

$$\begin{aligned}u_i = -\frac{1-\upsilon^2}{\pi}\sum_{k=1}^{N}\sigma_k\Bigg\{&\Theta\left(\frac{|\mathbf{X}_i - \mathbf{X}'_k|}{b}\right)\frac{1}{E_\infty}\int_{D_k}\frac{1}{|\mathbf{X}_i - \mathbf{X}'_k|} + \int_0^{+\infty}\mathrm{d}\tau\, C(\tau) \\ &\int_0^{+\infty}\mathrm{d}z\, \frac{1}{|\mathbf{X}_i + \mathbf{u}_d\tau z - \mathbf{X}'_k|}\Theta\left(\frac{|\mathbf{X}_i + \mathbf{u}_d\tau z - \mathbf{X}'_k|}{b}\right)\exp(-z)\Bigg\}\end{aligned} \tag{8}$$

where the terms $\int_{D_k} \mathrm{d}^2X'\, |\mathbf{X}_i - \mathbf{X}'|^{-1}$ and $\int_{D_k} \mathrm{d}^2X'\, |\mathbf{X}_i + \mathbf{u}_d\tau z - \mathbf{X}'|^{-1}$ can be easily calculated by exploiting Love's solution for elastic

DOI: 10.1021/acsami.7b09381
ACS Appl. Mater. Interfaces 2017, 9, 42287−42295

materials,[35] as shown in ref 36. In this way, the problem is reduced to a vectorial linear relation:

$$u_i = L_{ik}(\mathbf{u}_d)\sigma_k \tag{9}$$

where the response matrix $L_{ik}(\mathbf{u}_d)$ parametrically depends on the velocity $\mathbf{u}_d$. We observe that the total load acting on the system F_n is equal to $F_n = D_k\sum_{k=1}^{N}\sigma_k$ with the D_k being the area of each square cell.

Now, we can focus on the second equation, which is related to the fluid dynamics of the problem. We can assume all of the commonly employed assumptions are valid when dealing with soft lubrication, and in particular, we assume no-slip boundary conditions at both solids' interface. Let us, then, introduce the Reynolds equations, whose general form can be written as follows (see refs 18 and 19):

$$\frac{\partial \rho h}{\partial t} + \nabla\cdot(\rho h\mathbf{U}) = \nabla\cdot\left(\frac{\rho h^3}{12\eta}\nabla\sigma\right) \tag{10}$$

where $\mathbf{U}$ is the entrainment speed, i.e., the mean surface velocity that for the system depicted in Figure 2 is equal to $\mathbf{U} = (\mathbf{u}_b + \mathbf{u}_d)/2$, ρ is the density (which here is considered constant), η is the fluid viscosity, and h is the film thickness. The latter quantity can be easily related to the normal displacement of the deformable surface u, and specifically, $h(x, y) = h_0 + s(x, y) + u(x, y)$ with h_0 and $s(x, y)$ being, respectively, a rigid motion constant and the separation due to the undeformed geometry of the contacting surfaces. For the tribosystem studied in this paper and sketched in Figure 2, $s(x, y)$ is equal to $s(x, y) = R - (R - x^2 - y^2)^{1/2}$ with R being the radius of the sphere.

Given the steady-state conditions of our study, eq 10 simplifies since the time derivative vanishes and is, then, solved by means of a finite different scheme, whose nodes are equally spaced in the computational domain and correspond to the centers of the boundary elements previously defined for the solid problem. Indeed, such a procedure, where the differential terms in eq 10 are discretized with central finite differences,[18,19] allows us to reduce eq 10 to the following linear system:

$$h_i = R_{ik}(\mathbf{U}, \mu)\sigma_k \tag{11}$$

Ultimately, the problem consists of coupling the solid mechanics and fluid dynamics[18−20] and, consequently, of finding the pressure distribution that satisfies, at the same time, both eqs 9 and 11. An iterative scheme is adopted to solve the system formed by these two equations provided in vector form. Basically, at each iteration, given the estimation of the film thickness $\tilde{h}_i$ computed at the previous iteration, eq 11 is inverted to calculate an estimated stress field $\tilde{\sigma}_k$, which then is inputted in eq 9 to obtain the new viscoelastic deformation field $\tilde{u}_i$ and, consequently, the film thickness to employ at the next iteration. The iterative procedure, properly under-relaxed by means of the Aitken acceleration approach (see, e.g., ref 19), continues until film thickness and pressure distributions numerically converge in two consecutive iterations. Furthermore, with regards to the inversion of eq 9, in order to speed up the solving procedure, we may observe that the matrix R_{ik} is pentadiagonal thanks to the central finite difference discretization, and consequently, we may implement a direct solver which requires storing only the nonzero elements of the matrix R_{ik}.[37] The main advantage is the possibility of implementing a fine mesh and, at the same time, obtaining fast computational times. Once the problem is fully solved in terms of pressure distribution and deformations, it is straightforward to calculate the total friction as the sum of the viscoelastic hysteretic term[11] and the contribution coming from the fluid losses.[18]

Incidentally, we observe that, as usually done when dealing with numerical methods and, in particular, in lubrication problems, in this paper, the outcomes of the methodology are reported in dimensionless form. To this aim, we note that the characteristic length of the problem is the radius R: Consequently, when considering the film thickness h (and all deformations and quantities defined using units of length), we will look at the ratio h/R. Furthermore, when we have to analyze the stress distribution σ, it is convenient to make such a quantity dimensionless and write it as σ/E_0, by introducing the rubbery elastic modulus E_0.[11] Such a modulus is, then, employed as reference for quantities characterized by units of stress. As a consequence, the normal dimensionless load will be $F_n/(R^2E_0)$. Finally, to introduce a dimensionless speed ξ, we compare two time scales: The first one is a characteristic relaxation time τ of the material and the second one is the time employed by the fluid to cover the length R with the speed U.[11] Then, ξ is equal to $\xi = U\tau/R$. Finally, to deal with the viscosity η, we employ the dimensionless group $\eta UR/F_n$, that is, the so-called Hersey number.

3. RESULTS AND DISCUSSION

3.1. Film Thickness and Interfacial Pressure Distribution. We focus on the description of the physics governing the lubrication of a rigid sphere in pure rolling over a viscoelastic half-space. Consequently, the slide−roll ratio SRR, defined as $\mathrm{SRR} = (u_b - u_d)/((u_b + u_d)/2)$ with u_b and u_d being the speed of the sphere and of the disc, respectively, is set to zero.

Although these two conditions, i.e., the layer assumed as a half-space and the SRR being equal to zero, can be seen as a simplification with respect to the general formulation, they are only used here to reduce the number of parameters and show the effect of viscoelasticity in one of the simplest possible configurations. Furthermore, as a starting point and again in order to show the main peculiarities of lubricated viscoelastic response using a simple material model, we employ a one relaxation time material with a ratio E_∞/E_0 equal to $E_\infty/E_0 = 100$ and several different values of the relaxation time τ. Without loss of generality and for illustration purposes, all the calculations are carried out for a constant dimensionless normal load $F_n/(R^2E_0) = 8.5 \times 10^2$.

Now, by employing the numerical methodology described above, we can calculate how the pressure distribution and the film thickness depend on the dimensionless speed $\xi = U\tau/R$, where the fluid entrainment speed U is equal, in pure rolling conditions, to u_d. As shown in Figure 3, for very low values of ξ, the deformable solid is in the elastic rubbery region and behaves, consequently, as a soft elastic body: No viscoelastic effect is present. When looking at the lubricating film, as expected (see, e.g., refs 18 and 22), we observe an almost perfectly circular shape, and because of the flow conservation, a minimum at the fluid outlet can be observed. This is particularly evident in Figure 4, where both the fluid meatus and the normal stress distribution are plotted at the centerline of the contact depicted in Figure 3. Indeed, for $\xi = 0.005$, we notice a Hertzian-like pressure distribution, typical of low pressure contacts and iso-viscous fluids.[18]

However, a very different story has to be told when the speed is increased. Indeed the contact zone (i.e., the region delimited by low film and high pressure) gradually decreases its size and, most importantly, evolves toward a shape that is increasingly far from a circle and is affected by a sharp shrinkage at the fluid outlet. In Figure 3, the contour plots of the pressure clearly show this trend; as emphasized upon focus on the centerline in Figure 4, there exists a stress peak that increases with the speed and produces, ultimately, a strong asymmetry toward the contact inlet. Interestingly, such changes produce an additional local minimum in the fluid film: With an increase in the speed, this effect becomes predominant, and the absolute film thickness minimum moves from the flow outlet to the inlet. This is in agreement with recent experimental evidence;[23,24] however, this is certainly not intuitive and might come as a surprise for researchers familiar with classic lubrication models[18] and would be inadmissible if the rheology of the contacting solids were not to be considered. Hence, further

DOI: 10.1021/acsami.7b09381
ACS Appl. Mater. Interfaces 2017, 9, 42287−42295

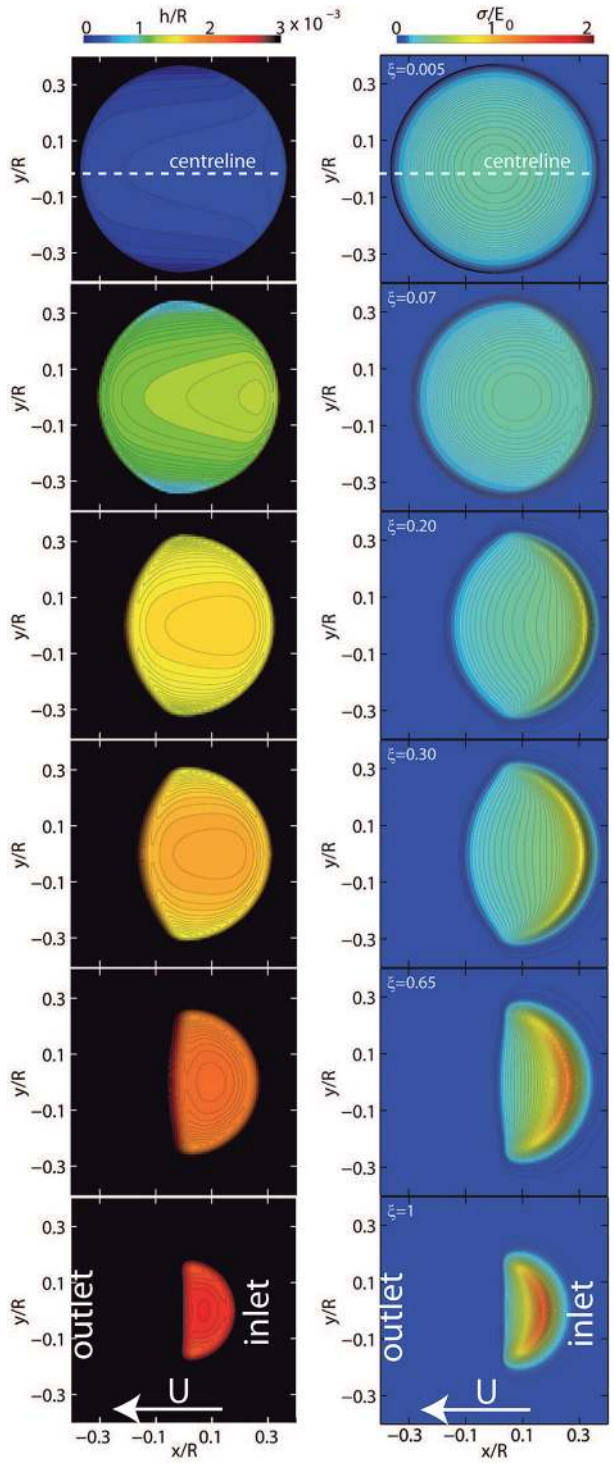

Figure 3. Contour plots of the film thickness (left) and the pressure distribution (right) predicted for a normal load of $F_n/(R^2E_0) = 8.5 \times 10^2$ and different values of the dimensionless speed ξ. Calculations are carried out for a viscoelastic half-space with a glass modulus $E_\infty = 10^8$ Pa, a ratio $E_\infty/E_0 = 100$, and a relaxation time $\tau = 0.01$ s, in contact with a sphere with a radius $R = 0.02$ m. The fluid has a constant viscosity equal to $\eta = 1$ Pa s.

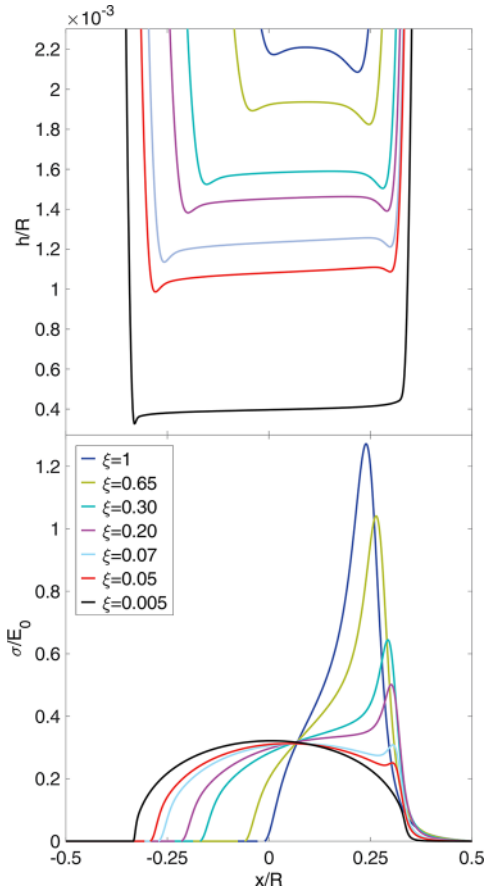

Figure 4. Film thickness (top) and pressure distribution (bottom) measured at the centerline of the contact ($y/R = 0$) for a normal load of $F_n/(R^2E_0) = 8.5 \times 10^2$ and different values of the dimensionless speed ξ.

considerations must be made to corroborate and explain these trends.

First of all, let us observe what happens in dry conditions when a rigid ball moves in rolling or sliding contact over a viscoelastic half-space. As shown in ref 11, the contact pressure has a peak at the leading edge, where the material has not been previously in contact with the rigid punch, and is smaller at the trailing edge, where the viscoelastic solid has been deformed and has not yet fully relaxed. Such a pressure field produces a contact area that is asymmetric and has a marked shrinkage at the trailing edge. When a fluid is inserted between the rigid punch and the viscoelastic layer, a similar mechanism occurs: At the flow inlet, i.e., where the lubricant is "sucked in", the viscoelastic material is basically undeformed; on the contrary, at the outlet, where the lubricant exits the contact region, the solid is still relaxing. This can be seen very clearly in Figure 5, where the viscoelastic displacement $u(x, y)$ is plotted for different values of the dimensionless speed ξ. As a consequence, similarly to what happens in dry conditions, larger pressure values have to be expected toward the inlet rather than at the flow outlet. A shrunk nonsymmetric film thickness and a minimum value at the inlet correspond to such a pressure distribution.

Furthermore, experimental comparisons with numerical results can be carried out by employing the same experimental setup shown in ref 23. This is based on the optical interferometry. Such a technique is normally used to detect the fluid film between two lubricated bodies: Fundamentally, light is shone into the lubricated contact through a transparent body, that is, usually glass or sapphire. Some of this light is reflected from the lower surface of the transparent disc while some passes through the lubricating film and is reflected on its turn from the reflective ball surface, which is usually steel.

DOI: 10.1021/acsami.7b09381
ACS Appl. Mater. Interfaces 2017, 9, 42287−42295

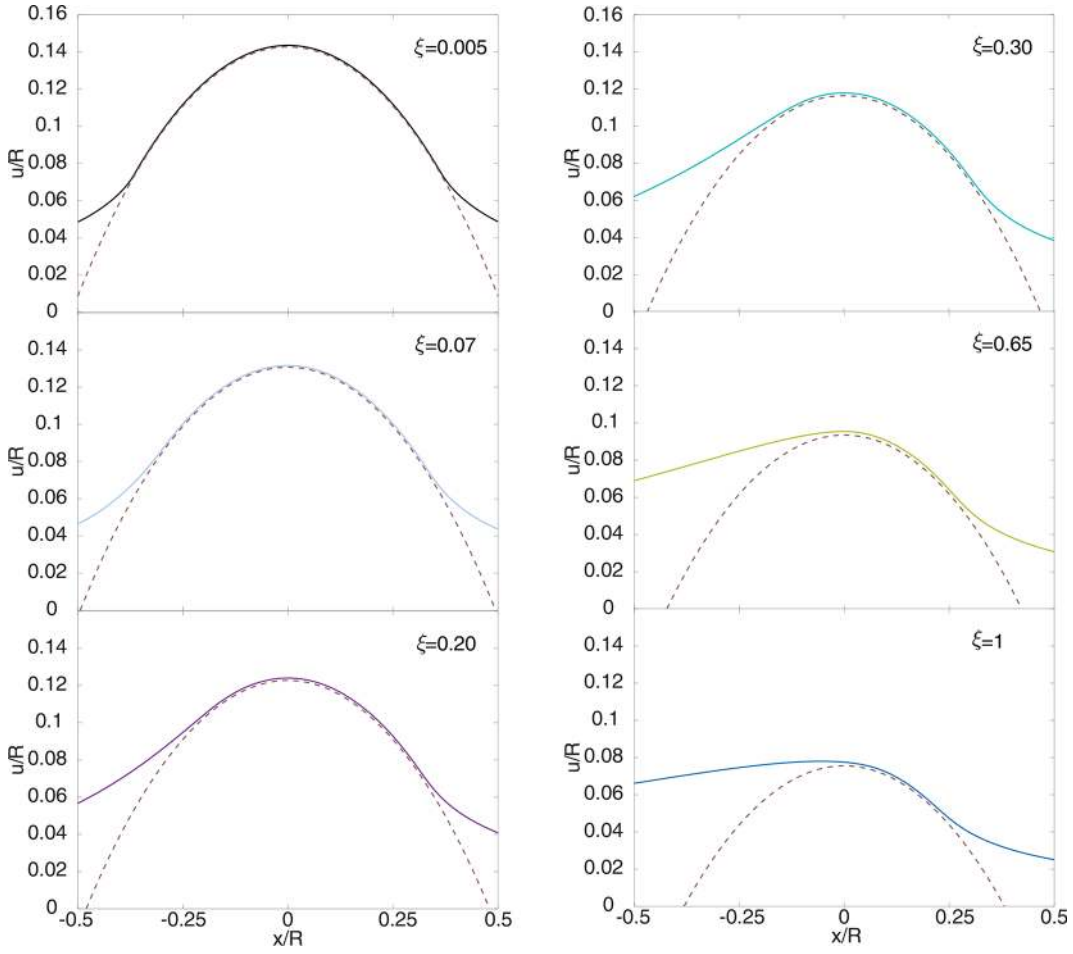

Figure 5. Displacement distribution $u(x, y)$ for different values of the dimensionless speed ξ. Dotted lines refer to the position of the rigid punch.

When the two light beams recombine, they interfere in a way that depends on the path difference between them and, consequently, on the lubricant film thickness. Such an experimental setup has been applied successfully to transparent poly(methyl methacrylate) (PMMA) disks by applying a semireflective chromium coating on the polymeric material. As for the lubricant, an additive-free base fluid, of a gas-to-liquid origin and corresponding broadly to API group IIIÃ, is employed. More details, including the viscometric properties of the fluid, can be found in ref 23. With regards to the disk material, PMMA is a viscoelastic polymer whose properties have been obtained by means of dynamic mechanical analysis performed on the Q800 dynamic mechanical analyzer (DMA) manufactured by TA Instruments (see the Supporting Information for more details). In Figure 6, results show a good qualitative and quantitative agreement between the contour map of the film thickness experimentally measured at the temperature of T = 40 °C and the equivalent contour plot obtained numerically. A marked deviation from the circular shape of the contact zone, which cannot be captured using classical elasto-hydrodynamic lubrication, and neglecting the effect of the solid rheology, is clearly shown. As shown also in ref 23, and coherently with the theoretical framework so far developed, such an effect and, in particular, the shrinkage at the flow inlet are strongly dependent on the entrainment speed.

A more direct quantitative analysis of the film at the contact centerline, carried out for different values of entrainment speed and for a normal load of F_n = 15 N, shows a good agreement

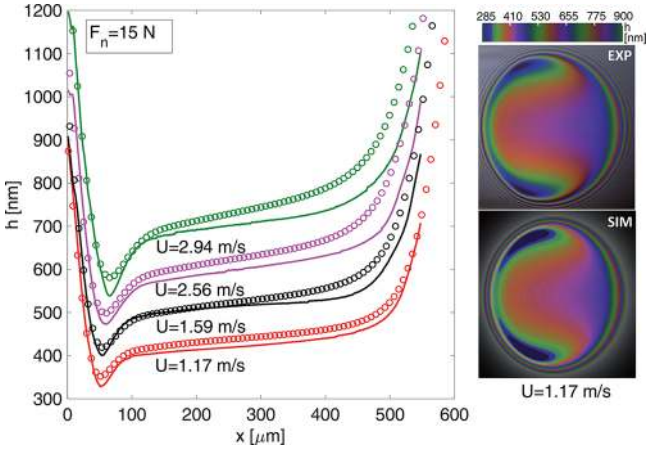

Figure 6. Interferometer map (top right) and numerical contour plot (bottom right) of film thickness for a normal PMMA sample subjected to a normal load of F_n = 15 N and an entrainment speed U = 1.17 m/s. Comparison between numerical predictions and experimental outcomes at the centerline (y/R = 0) for different values of the entrainment speed (left).

with the numerical outcomes with discrepancies always below 8%. The observation of the pronounced shrinkage of the lubricating film and the accuracy of the quantitative comparison between experimental and numerical results highlight the role that might be played by solid viscoelasticity. However, at the same time, in the current experimental setup, viscoelastic effects

DOI: 10.1021/acsami.7b09381
ACS Appl. Mater. Interfaces 2017, 9, 42287−42295

are not as strong as those observed, for example, in Figures 3 and 4. Indeed, the experimental evidence and the numerical results presented so far suggest that viscoelastic effects can be more or less pronounced depending on the fluid viscosity and the frequency/speed range in which solid viscoelasticity is prominent for the specific material under investigation. In other words, the rheologies of the fluid and of the solid undergo a complex interplay, with different levels of coupling between the fluid film and the deformation of the solid bodies, which leads to different lubrication scenarios and frictional responses. Such an interplay is discussed next.

3.2. Solid Viscoelasticity and Fluid Viscosity: A Coupling Criterion. To quantify the coupling and the interaction between viscoelastic deformations in the solid and fluid film, let us primarily focus on the two parameters that govern the phenomenon. Starting from the aspects linked to the dynamics of the fluid, all the properties and, in particular, friction, which will be used as a measure of the effect that the coupling has on dissipation, are determined by the Hersey number, $\eta UR/F_n$.[18] With regards to the solid, we have a frequency where viscoelastic losses and, specifically, the loss tangent reach a maximum: In the very simple case of a one relaxation time material, such a frequency, which maximizes the ratio $\mathrm{Im}[E(\omega)]/|E(\omega)|$, can be estimated analytically and is equal to $\omega_{cr} \approx \pi^{-1}\sqrt{E_\infty/E_0}$.[11] The critical disc speed associated with this frequency is equal to $u_d|_{cr} \approx \omega_{cr}R/\tau$, and therefore, since in rolling conditions $U = u_d$, the critical entrainment speed can be estimated as $U_{cr} = (R/\pi\tau)\sqrt{E_\infty/E_0}$.

Now, it is straightforward to observe that, given a constant normal load, when we increase the speed, the minimum and the mean film thickness increase, and as expected from classical lubrication theory, once we pass from the elasto-hydrodynamic to the hydrodynamic regime, any deformation in the contacting solids tends to decrease. As shown also in Figure 5, when the deformable layer is viscoelastic, the situation is similar to the only difference that, by increasing the speed, the solid become stiffer until we reach the elastic glassy regime where $E(\omega)$ is equal to E_∞. Therefore, the transition between a deformable regime, that we could now define as visco-elasto-hydrodynamic lubrication (VEHL), to the hydrodynamic behavior can be even faster. Now, given a viscoelastic solid, we may wonder what happens if, for a given load, U_{cr} falls into the hydrodynamic region, and consequently, no deformation occurs at the critical speed: Simply, no viscoelastic effect will be observed. We have an elasto-hydrodynamic regime (the solid behaves elastically with a rubber modulus E_0) followed by a hydrodynamic regime at larger speeds. It emerges that viscoelasticity is a necessary, but not sufficient, condition to see a marked deviation from classical EHL conditions. For observation of the visco-elasto-hydrodynamic regime, the solid deformation at the critical speed U_{cr} has to be large and comparable with the film thickness. This observation leads to the introduction of the following coupling parameter:

$$\Gamma = \frac{h_{hydro}}{\delta_{cr}} \tag{12}$$

with h_{hydro} and δ_{cr} being, respectively, the minimum film thickness in hydrostatic conditions and the solid penetration at the critical speed. For a VEHL regime, $\Gamma \approx 1$. The minimum hydrostatic film thickness can be found solving the Reynolds equations and, for our configuration, as shown in ref 38, is equal to $h_{hydro} = RH_{hydro}$ with H_{hydro} being a dimensionless quantity equal to $H_{hydro} = \alpha(\eta U_{cr}R/F_n)^2$ with α a constant numerically found equal to $\alpha \approx 1.3 \times 10^2$. The penetration δ_{cr} can be approximately estimated using the Hertzian relations as $\delta_{cr} \approx (9F_n^2/16R(E^*(\omega_{cr}))^2)$.

This is a powerful tool, as evaluating Γ allows, given the viscoelastic modulus $E(\omega)$ and the fluid viscosity η, determination of if a visco-elasto-hydrodynamic behavior has to be expected in first order approximation for materials governed by linear viscoelasticity. To show the effects induced by the VEHL regime, let us focus on the friction force, which is the sum of the fluid contribution and the viscoelastic dissipation in the solid. Incidentally, we observe that the role of the roughness is out of the scope of this paper since it would play a significant role in the so-called boundary and mixed regimes and would not influence the regimes in which the fluid film is fully formed, which are the subject of our investigation. Now, if viscoelastic effects are not significant we have a transition between EHL and hydrodynamic (HD) regimes regulated by the Stribeck curve: At very low speeds, the friction tends to zero, whereas, at larger speeds, we have a linear dependence between the friction and the logarithm of the speed. The situation is different when viscoelasticity is significant since viscoelastic hysteresis adds a source of dissipation and modifies the friction curve. This appears very clearly in Figure 7 where

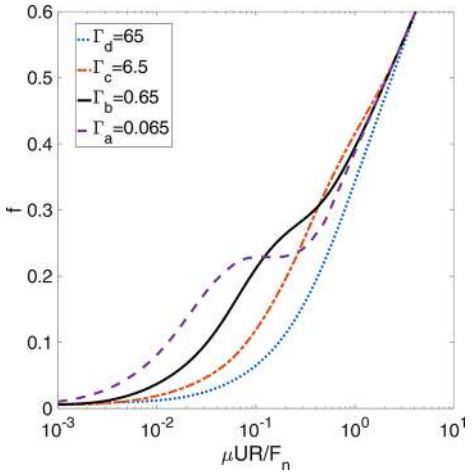

Figure 7. Friction coefficient f as a function of the speed for a dimensionless load equal to $F_n/(R^2E_0) = 8.5 \times 10^2$ and different values of the parameter Γ: $\Gamma_a = 0.065$, $\Gamma_b = 0.65$, $\Gamma_c = 6.5$, and $\Gamma_d = 65$. They have been obtained by employing the following four different values of τ: $\tau_a = 10^{-2}$ s, $\tau_b = 3.5 \times 10^{-2}$ s, $\tau_c = 10^{-3}$ s, and $\tau_d = 10^{-4}$ s.

the coefficient of friction is plotted for a material whose viscoelasticity is characterized by one relaxation time material, with a ratio $E_\infty/E_0 = 100$, and four different values of relaxation time. By changing the relaxation time, we are shifting the viscoelastic spectrum, thus obtaining four different values of Γ: $\Gamma_a = 0.065$, $\Gamma_b = 0.65$, $\Gamma_c = 6.5$, and $\Gamma_d = 65$. As shown in Figure 7, when Γ is small, we have a deviation from the Stribeck curve with a marked "bump" due to the viscoelastic hysteretic contribution; for larger values of τ and, consequently, of Γ, the viscoelastic friction peak moves toward larger speeds and, then, as explained before, decreases its intensity until it disappears. Indeed, for $\Gamma = \Gamma_d$, we have a standard Stribeck curve: Specifically, for low speeds, we have an EHL region, where the body deforms elastically with a modulus equal to the rubber

DOI: 10.1021/acsami.7b09381
ACS Appl. Mater. Interfaces 2017, 9, 42287−42295

modulus E_0, and then, for larger values of the speed, there is the HD regime where the solid would be potentially able to show viscoelastic effects; however, since the pressure is not large enough to significantly deform the material, no energy dissipation occurs.

As expected, and consistent with the proposed theoretical framework, all the four curves tend to collapse at low speed (low Hersey number) to a soft-EHL behavior, and at large speeds (high Hersey number) we find the same hydrodynamic regime, which is dictated only by the ball geometry and the fluid viscosity.

4. CONCLUSIONS

In this study, we have shown that when dealing with the lubrication of soft solids that exhibit a viscoelastic rheology, the role of viscoelasticity has to be carefully accounted for since it can be responsible for phenomena that cannot be predicted by classical lubrication models. Indeed, it has been shown that the rheology of the solid can have profound effects on both the fluid film thickness and pressure distribution, in turn affecting the capacity to predict the behavior of soft systems under lubricated conditions. Indeed, the lubricating film shows a marked shrinkage at the outlet with a possible additional minimum point at the inlet, where the pressure distribution presents a peak. Looking at friction and dissipation, viscoelastic hysteretic contributions must be added to fluid viscous losses, leading to friction−speed dependencies different from those conventionally encountered in the Stribeck curve. Such a scenario may provide a theoretical explanation to a number of phenomena, like, for example, the unexpected rupture of the lubricating film at the flow inlet shown in ref 24, and is confirmed experimentally by carrying out an interferometer analysis on PMMA samples.

What emerges from this investigation is that, given a viscoelastic material, viscoelastic effects may be more or less marked depending on the degree of coupling between the rheologies of the fluid and the solid: If the maximum loss tangent corresponds to a speed where no significant deformation occurs, i.e., a speed that falls into a hydrodynamic regime, no visco-elasto-hydrodynamic regime can be observed. A new criterion has been provided to assess the effect that the interplay between solid and fluid rheologies has in soft contacts: This can be effectively used to design systems (e.g., for industrial components, like rubber bearings and seals, bioinspired devices, and soft electronics) in which the viscoelastic effects need to be controlled through careful development of new materials and tuning of their properties.

■ ASSOCIATED CONTENT

Supporting Information

The Supporting Information is available free of charge on the ACS Publications website at DOI: 10.1021/acsami.7b09381.

Detailed description of the mechanical characterization carried out for PMMA employed in the comparison between the experimental outcomes and the numerical simulations (PDF)

■ AUTHOR INFORMATION

Corresponding Author

*E-mail: carmine.putignano@poliba.it.

ORCID

Carmine Putignano: 0000-0001-6225-9630

Daniele Dini: 0000-0002-5518-499X

Notes

The authors declare no competing financial interest.

Data reported in this paper can be obtained upon request by emailing tribology@imperial.ac.uk.

■ ACKNOWLEDGMENTS

The authors thank Dr. N. Marx for fruitful discussions on the experimental technique used in the paper. C.P. and D.D. also acknowledge the support of the Marie Curie Intra-European Fellowship SOFTMECH (Grant 622632) and the EPSRC Established Career Fellowship (EP/N025954/1).

■ REFERENCES

(1) Ahn, B. K.; Lee, D. W.; Israelachvili, J. N.; Waite, J. H. Surface-initiated self-healing of polymers in aqueous media. *Nat. Mater.* **2014**, *13*, 867−872.

(2) Olabisi, O., Adewale, K. *Handbook of Thermoplastics*; CRC Press, 2016.

(3) Bao, G.; Suresh, S. Cell and molecular mechanics of biological materials. *Nat. Mater.* **2003**, *2*, 715−725.

(4) Licup, A. J.; Münster, S.; Sharma, A.; Sheinman, M.; Jawerth, L. M.; Fabry, B.; Weitz, D.; MacKintosh, F. C. Stress controls the mechanics of collagen networks. *Proc. Natl. Acad. Sci. U. S. A.* **2016**, *112*, 31.

(5) Heepe, L.; Gorb, S. N. Biologically Inspired Mushroom-Shaped Adhesive Microstructures. *Annu. Rev. Mater. Res.* **2014**, *44*, 173−203.

(6) Pastewka, L.; Robbins, M. O. Contact between roughsurfaces and a criterion for macroscopic adhesion. *Proc. Natl. Acad. Sci. U. S. A.* **2014**, *111* (9), 3298−3303.

(7) Rus, D.; Tolley, M. T. Design, fabrication and control of soft robots. *Nature* **2015**, *521*, 467−475.

(8) Hunter, S. C. The rolling contact of a rigid cylinder with a viscoelastic half space. *J. Appl. Mech.* **1961**, *28*, 611−617.

(9) Persson, B. N. J.; Albohr, O.; Tartaglino, U.; Volokitin, A. I.; Tosatti, E. On the nature of surface roughness with application tocontact mechanics, sealing, rubber friction and adhesion. *J. Phys.: Condens. Matter* **2005**, *17*, 1.

(10) Dapp, W. B.; Lücke, A.; Persson, B. N. J.; Müser, M. H. Self-affine elastic contacts: Percolation and leakage. *Phys. Rev. Lett.* **2012**, *108* (24), 244301.

(11) Carbone, G.; Putignano, C. A novel methodology to predict sliding/rolling friction in viscoelastic materials: theory and experiments. *J. Mech. Phys. Solids* **2013**, *61* (8), 1822−1834.

(12) Grosch, K. A. The Relation between the Friction and Visco-Elastic Properties of Rubber. *Proc. R. Soc. London, Ser. A* **1963**, *274* (1356), 21−39.

(13) Putignano, C.; Reddyhoff, T.; Carbone, G.; Dini, D. Experimental investigation of viscoelastic rolling contacts: a comparison with theory. *Tribol. Lett.* **2013**, *51*, 105−113.

(14) Scaraggi, M.; Persson, B. N. J. Theory of viscoelastic lubrication. *Tribol. Int.* **2014**, *72*, 118−130.

(15) Hooke, C. J.; Huang, P. Elastohydrodynamic lubrication of soft viscoelastic materials in line contact. *Proc. Inst. Mech. Eng., Part J* **1997**, *211*, 185.

(16) Elsharkawy, A. A. Visco-elastohydrodynamic lubrication of line contacts. *Wear* **1996**, *199*, 45−53.

(17) Pandey, A.; Karpitschka, S.; Venner, C. H.; Snoeijer, J. H. Lubrication of soft viscoelastic solids. *J. Fluid Mech.* **2016**, *799*, 433−447.

(18) Hamrock, B. J., Schmid, S. R., Jacobson, B. O. *Fundamentals of Fluid Film Lubrication*; CRC Press, 2004.

(19) Venner, C. H., Lubrecht, A. A. *Multilevel Methods in Lubrication, Tribology Series*; Dowson, D., Ed.; Elsevier, 2000; Vol. 37.

(20) Snoeijer, J. H.; Eggers, J.; Venner, C. H. Similarity theory of lubricated Hertzian contacts. *Phys. Fluids* **2013**, *25* (10), 101705.

(21) Stupkiewicz, S.; Lengiewicz, J.; Sadowski, P.; Kucharski, S. Finite deformation effects in soft elastohydrodynamic lubrication problems. *Tribol. Int.* **2016**, *93*, 511−522.
(22) Bowden, F. P., Tabor, D. *The Friction and Lubrication of Solids*; Clarendon Press, 2001.
(23) Marx, N.; Guegan, J.; Spikes, H. A. Elastohydrodynamic film thickness of soft EHL contacts using optical interferometry. *Tribol. Int.* **2016**, *99*, 267−277.
(24) Hutt, W.; Persson, B. N. J. Soft matter dynamics: Accelerated fluid squeeze-out during slip. *J. Chem. Phys.* **2016**, *144*, 124903.
(25) Selway, N.; Chan, V.; Stokes, J. R. Influence of fluid viscosity and wetting on multiscale viscoelastic lubrication in soft tribological contacts. *Soft Matter* **2017**, *13*, 1702−1715.
(26) Endlein, T.; Barnes, W. J. P.; Samuel, D. S.; Crawford, N. A.; Biaw, A. B.; Grafe, U. Sticking under Wet Conditions: The Remarkable Attachment Abilities of the Torrent Frog, Staurois guttatus. *PLoS One* **2013**, *8*, e73810.
(27) André, T.; Lévesque, V.; Hayward, V.; Lefèvre, P.; Thonnard, J.-L. Effect of skin hydration on the dynamics of fingertip gripping contact. *J. R. Soc., Interface* **2011**, *8*, 1574−1583.
(28) Putignano, C.; Afferrante, L.; Carbone, G.; Demelio, G. The influence of the statistical properties of self-affine surfaces in elastic contact: a numerical investigation. *J. Mech. Phys. Solids* **2012**, *60* (5), 973−982.
(29) Putignano, C.; Carbone, G.; Dini, D. Theory of reciprocating contact for viscoelastic solids. *Phys. Rev. E: Stat. Phys., Plasmas, Fluids, Relat. Interdiscip. Top.* **2016**, *93*, 043003.
(30) Christensen, R. M. *Theory of viscoelasticity*; Academic Press: New York, 1971.
(31) Williams, M. L.; Landel, R. F.; Ferry, J. D. *J. Am. Chem. Soc.* **1955**, *77*, 3701.
(32) Carbone, G.; Mangialardi, L. Adhesion and friction of an elastic half-space in contact with a slightly wavy rigid surface. *J. Mech. Phys. Solids* **2004**, *52* (6), 1267−1287.
(33) Putignano, C.; Carbone, G.; Dini, D. Mechanics of Rough Contactsin Elastic and Viscoelastic Thin Layers. *Int. J. Solids Struct.* **2015**, *69−70*, 507−517.
(34) Putignano, C.; Dapp, W.; Muser, M. A GFMD approach to themechanical contact between thin elastic sheets and randomly rough surfaces. *Biomimetics* **2016**, *1* (1), 7.
(35) Johnson, K. L. J. *Contact Mechanics*; Cambridge University Press, 1985.
(36) Putignano, C.; Afferrante, L.; Carbone, G.; Demelio, G. A new efficient numerical method for contact mechanics of rough surfaces. *Int. J. Solids Struct.* **2012**, *49* (2), 338−343.
(37) Schenk, O.; Gärtner, K. Solving unsymmetric sparsesystems of linear equations with PARDISO. *Future Generation Computer Systems* **2004**, *20* (3), 475−487.
(38) Esfahanian, M.; Hamrock, B. J. Fluid-Film Lubrication Regimes Revisited. *Tribol. Trans.* **1991**, *34* (4), 628−632.

DOI: 10.1021/acsami.7b09381
ACS Appl. Mater. Interfaces 2017, 9, 42287−42295